

RESEARCH ARTICLE

Simulation of angiogenesis in three dimensions: Application to cerebral cortex

Jonathan P. Alberding¹, Timothy W. Secomb^{1,2*}¹ BIO5 Institute, University of Arizona, Tucson, Arizona, United States of America, ² Department of Physiology, University of Arizona, Tucson, Arizona, United States of America* secomb@u.arizona.edu

OPEN ACCESS

Citation: Alberding JP, Secomb TW (2021) Simulation of angiogenesis in three dimensions: Application to cerebral cortex. PLoS Comput Biol 17(6): e1009164. <https://doi.org/10.1371/journal.pcbi.1009164>

Editor: Philip K. Maini, Oxford, UNITED KINGDOM

Received: January 12, 2021

Accepted: June 8, 2021

Published: June 25, 2021

Copyright: © 2021 Alberding, Secomb. This is an open access article distributed under the terms of the [Creative Commons Attribution License](https://creativecommons.org/licenses/by/4.0/), which permits unrestricted use, distribution, and reproduction in any medium, provided the original author and source are credited.

Data Availability Statement: All computer programs and data files used to generate the results are available from GitHub <https://github.com/secomb>.

Funding: This work was supported by National Institutes of Health Grants R01 HL034555 (TWS) and U01 HL133362 (TWS). www.nih.gov. The funders had no role in study design, data collection and analysis, decision to publish, or preparation of the manuscript.

Competing interests: The authors have declared that no competing interests exist.

Abstract

The vasculature is a dynamic structure, growing and regressing in response to embryonic development, growth, changing physiological demands, wound healing, tumor growth and other stimuli. At the microvascular level, network geometry is not predetermined, but emerges as a result of biological responses of each vessel to the stimuli that it receives. These responses may be summarized as angiogenesis, remodeling and pruning. Previous theoretical simulations have shown how two-dimensional vascular patterns generated by these processes in the mesentery are consistent with experimental observations. During early development of the brain, a mesh-like network of vessels is formed on the surface of the cerebral cortex. This network then forms branches into the cortex, forming a three-dimensional network throughout its thickness. Here, a theoretical model is presented for this process, based on known or hypothesized vascular response mechanisms together with experimentally obtained information on the structure and hemodynamics of the mouse cerebral cortex. According to this model, essential components of the system include sensing of oxygen levels in the midrange of partial pressures and conducted responses in vessel walls that propagate information about metabolic needs of the tissue to upstream segments of the network. The model provides insights into the effects of deficits in vascular response mechanisms, and can be used to generate physiologically realistic microvascular network structures.

Author summary

During brain development, a two-dimensional mesh-like network of flowing blood vessels spreads over the surface of the growing cortex. Branches from this network penetrate the cortex and connect, forming a three-dimensional network throughout the tissue. Arterio-venous connections on the surface regress, and flow is directed to the interior, so that the cortex is well supplied with oxygen to meet the metabolic demands of neural function. This study aims to better understand how vascular growth, structural remodeling and pruning in response to local metabolic and hemodynamic stimuli generate microvascular networks that meet functional demands. A theoretical model is used to simulate angiogenesis in three dimensions. In this model, a growth factor is generated in tissue at a rate that

depends on local oxygen level, and diffuses to existing vessels, where it stimulates increase in diameter and formation of new sprouts if its level is high enough. These mechanisms, along with vascular responses to wall shear stress and pressure, result in networks with similar structural and oxygen transport characteristics to experimentally observed networks. The model shows that vascular responses to metabolic signals, including conducted responses propagated upstream along vessel walls, are essential for formation of adequate network structures. Impairment of conducted responses may contribute to cognitive decline with aging and neurodegenerative diseases.

Introduction

The effective functioning of the vascular system depends sensitively on its geometrical characteristics. The rate of convective transport by blood depends on the rate of blood flow, which is proportional to the fourth power of vessel diameter according to Poiseuille's law, for a given pressure gradient and viscosity [1]. Rates of diffusive transport of solutes between blood and surrounding tissue are proportional to the gradients in solute concentration, and therefore vary inversely with the distance that the solute must diffuse. In the case of oxygen transport, the maximum diffusion distance is very short, generally less than 100 μm [2], and so blood flow must pass very close to all parts of the tissue to ensure adequate oxygenation.

This sensitivity of mass transport to geometrical properties implies the need for tight control of vascular network structures in order to meet the functional needs of tissues. The question arises: what are the biological mechanisms that control the geometry of vascular networks? During embryonic development, the locations of the major arteries and veins are under tight genetic control. However, the vascular system contains more than 10^9 vessel segments, and individual control of their characteristics is clearly not feasible [3]. Moreover, the vasculature is capable of substantial growth and regression during a range of physiological processes such as exercise training, female reproductive cycle, wound healing and tumor growth. These considerations imply that blood vessels must exhibit a set of generic behaviors and responses, enabling them to self-assemble into well-organized networks that meet the needs of the tissue for transport of oxygen and other essential materials [3].

The overall goal of this work is to gain insight into these generic responses. The approach used is to develop biologically plausible hypotheses for the underlying mechanisms, perform theoretical simulations of angiogenesis and structural adaptation based on these hypotheses, and compare the characteristics of the resulting networks with experimental observations. Vascular structures vary greatly with tissue and species. Here, a specific observed network structure in the cerebral cortex of the mouse is used as a basis for comparison [4]. Geometrical, blood flow and oxygen transport properties of this network have been characterized [5], allowing a stringent assessment of results of simulated angiogenesis in this tissue. In previous work [6], we developed a model for angiogenesis in two dimensions based on observations of the rat mesentery, a thin sheet-like tissue. The cerebral cortex vasculature is inherently three-dimensional, and the development of a model for angiogenesis in three dimensions is an aim of the present work.

During the prenatal development of the rodent brain, a vascular plexus spreads over the surface of the neural tissue [7]. These vessels are referred to as the pial vasculature, because they are adjacent to the pia mater, the innermost membrane surrounding the brain tissue. Sprouting angiogenesis from this plexus generates vessels that invade the tissue, forming interconnections and providing perfusion to the developing brain. This begins around embryonic

day E9.5 in the mouse [8]. A notable aspect of this developmental process is the necessity for regression and pruning of arterial-venous connections in the surface plexus, which would otherwise shunt blood flow away from the interior of the tissue. In the present model, the initial condition includes a single blood flow pathway on the outer surface of the cortex, and the processes of sprouting angiogenesis, connection of sprouts to form new flow pathways, and pruning of surface arterial-venous connections are simulated.

The development of theoretical models for angiogenesis has been the subject of numerous previous studies. Much of this work has focused on the simulation of angiogenesis in solid tumors [9–21] and wound healing [22–24]. While these are important cases, the high degree of variability in the physiological environment and in the resulting network structures under pathological conditions makes it difficult to calibrate and test the resulting models. With regard to vascular growth in normal tissues, early development by vasculogenesis has been modeled [25,26] but relatively few models have been developed for vascular growth by sprouting angiogenesis in normal tissues [6,27,28]. Angiogenesis in the brain has been considered in the context of models of tumor growth [29] but normal vascular development in the cerebral cortex does not appear to have previously been modeled. The structure and hemodynamics of the mouse cortex microvasculature have been studied in detail [4,5], providing a basis for quantitative assessment of the models presented here.

The present approach is based on previously described concepts [6,30,31]. A dynamic model is used to simulate the development of the cortical vasculature. At successive time steps, the spatial distributions of oxygen and a diffusible growth factor are computed, where the production rate of growth factor depends on the local oxygen level. The responses of the vessel network to growth factor are simulated, including angiogenesis, structural adaptation and pruning (Fig 1A). The initial condition consists of a single flowing vessel lying on the surface of the cortex with two non-flowing sprouts (Fig 1B). This model provides insight into the roles that various biological mechanisms play in the generation of stable, functionally adequate network structures, and allows investigation of the effects of downregulating these mechanisms.

Methods

Tissue configuration and initial network structure

The simulated region of cortical tissue is a hexagonal prism with height 500 μm and width 300 μm , each side of the hexagon being 150 μm (Fig 1B). The shape is chosen to allow a hexagonally periodic network structure in the plane of the cortex. Any vessel that exits through one side of the hexagon is continued by a corresponding segment entering on the opposite side. Previous work [32] assumed cubic periodicity. The tissue volume (0.0294 mm^3) is large enough to include a representative vascular network including arterioles, capillaries and venules, while small enough to allow fast computations; computation time increases rapidly with the size of the domain. Parameter values are specified in Table 1.

The state of the system is computed at discrete time steps Δt . At each time step, the network is represented as a set of connected straight segments with defined positions, lengths, diameters and blood flow rates. In the initial configuration, blood flow across the upper surface of the tissue is driven by fixed pressures of 100 mmHg at the inflow node and 20 mmHg at the outflow node of a pial vessel. The partial pressure of oxygen (P_{O_2}) in the inflowing blood is set to 100 mmHg. This vessel includes a narrow upstream segment with fixed diameter of 7 μm and length 35 μm , to represent the flow resistance of upstream pial arteries and arterioles. The resulting initial flow rate is 40.2 nl/min.

A distinctive feature of the cortical vasculature is the arrangement of the penetrating arterioles and venules, which extend into the cortical tissue almost perpendicular to the pial surface

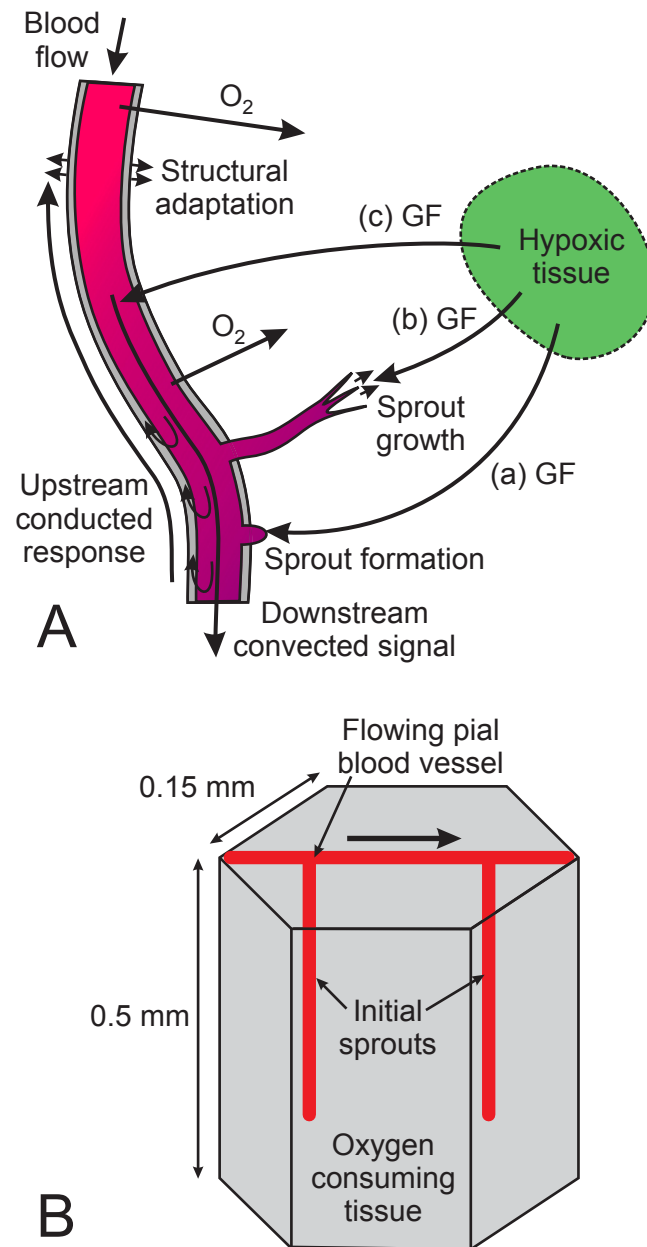


Fig 1. (A) Schematic representation of assumed mechanisms of vascular growth and adaptation. Vessels are assumed to respond to local GF concentration in three ways. (a) Existing vessels may develop sprouts if the GF level is above a threshold value. (b) Sprouts elongate with time and connect to other vessels to form flow pathways. The growth direction of each sprout is biased towards regions with higher GF levels. (c) GF reaching a vessel generates a metabolic stimulus that is distributed downstream along the vessel by convection and upstream by conducted responses in vessel walls. **(B) Definition of initial configuration.** A hexagonal tissue region is simulated, with periodic boundary conditions in the plane of the hexagon. The region forms part of a repeating structure to represent the cerebral cortex. The initial vascular configuration consists of a single flowing segment representing a pial vessel, and two perpendicular sprouts representing a penetrating arteriole and a penetrating venule. Flow direction in pial vessel is indicated by arrow.

<https://doi.org/10.1371/journal.pcbi.1009164.g001>

[33]. Distal vessels have more random orientations. To incorporate these features in the model, the initial condition includes two straight sprouts extending 400 μm into the tissue perpendicular to the pial vessel (Fig 1B).

Table 1. Reference parameters.

		Source
Blood oxygen parameters		
Maximal RBC oxygen concentration	$C_0 = 0.516 \text{ cm}^3 \text{O}_2 \text{ cm}^{-3}$	[36]
Effective oxygen solubility in blood	$\alpha_{eff} = 3.1 \times 10^{-5} \text{ cm}^3 \text{O}_2 \text{ cm}^{-3} \text{ mmHg}^{-1}$	[36]
Hill equation parameter	$P_{50} = 40.2 \text{ mmHg}$	[37]
Hill equation parameter	$n = 2.59$	[37]
Tissue oxygen parameters		
Krogh diffusion constant	$D_{O_2} \alpha = 9.375 \times 10^{-10} \text{ cm}^3 \text{O}_2 \text{ cm}^{-1} \text{ s}^{-1} \text{ mmHg}^{-1}$	[36]
Consumption rate	$M_0 = 7.5 \text{ cm}^3 \text{O}_2 (100 \text{ cm}^3)^{-1} \text{ min}^{-1}$	[5]
P_{O_2} at half-maximal consumption	$P_c = 10.5 \text{ mmHg}$	[38]
Growth factor parameters		
Diffusivity of GF	$D_{GF} = 2 \times 10^{-7} \text{ cm}^2 \text{ s}^{-1}$	*
Tissue GF degradation rate constant	$K_{GF} = 8 \times 10^{-3} \text{ s}^{-1}$	*
Maximal GF concentration	$C_{GF0} = 1$	**
Reference oxygen level for GF release	$P_{GF} = 40 \text{ mmHg}$	*
Exponent for GF release	$N_{GF} = 2.5$	*
Angiogenesis parameters		
Time step	$\Delta t = 0.05 \text{ day}$	
Diameter of new sprouts	$D_s = 8 \text{ }\mu\text{m}$	[39]
Threshold GF concentration for sprouting	$C_{th} = 0.7$	*
Constant in sprouting probability function	$C_{th50} = 0.5$	*
Maximum sprout formation probability	$k_p = 0.22 \text{ }\mu\text{m}^{-1} \text{ day}^{-1}$	*
Sprout growth rate	$V_g = 333 \text{ }\mu\text{m day}^{-1}$	*
Directional response to GF gradient	$k_{GF} = 20 \text{ }\mu\text{m}^{-1}$	*
Attraction constant to nearby vessels	$k_V = 1 \text{ }\mu\text{m}^{-1}$	*
Maximum vessel sensing distance	$R_{max} = 25 \text{ }\mu\text{m}$	[8]
Maximum vessel sensing angle	$\theta_{max} = \pi/3$	[6]
Variance of growth direction randomization	$\sigma_s = 0.05$	*
Vessel migration parameters		
Threshold for migration	$\lambda_t = 0.25$	*
Maximum migration velocity	$v_{max} = 80 \text{ }\mu\text{m day}^{-1}$	*
Structural adaptation parameters		
Structural adaptation time scale	$T = 1 \text{ day}$	*
Reference wall shear stress	$\tau_{ref} = 0.01 \text{ dyn cm}^{-2}$	†
Metabolic sensitivity	$k_m = 18$	*
Shrinking tendency	$k_s = 1.8$	*
Vessel permeability to GF (or GF product)	$\kappa_{GF} = 1$	**
Reference flow rate for metabolic signal	$Q_{ref} = 0.1 \text{ nl min}^{-1}$	†
Convected response saturation constant	$C_{GF50}^v = 200 \text{ }\mu\text{m}$	*
Conducted response saturation constant	$J_{c50} = 500 \text{ }\mu\text{m}$	*
Conducted response length constant	$L_c = 1.73 \text{ cm}$	[40]
Relative strength of conducted response	$S_c^{max} = 1$	**

*See text for discussion.

**Arbitrary units; set to 1.

†Small constant to avoid singular behavior.

<https://doi.org/10.1371/journal.pcbi.1009164.t001>

Flow rates

In the simulation of blood flow at each time step, the vessel network is represented as a set of segments connected at nodes [34,35]. Each segment has a flow resistance

$$R = \Delta P / Q = 128L\eta_{app} / (\pi D^4) \quad (1)$$

where ΔP is pressure drop, Q is flow rate, L is length, D is diameter, and η_{app} is apparent viscosity of blood, which depends on diameter and hematocrit [1,34]. The condition that the sum of the flows into each internal node is zero yields a set of linear equations for the nodal pressures [41], which is solved iteratively. Effects of phase separation at diverging bifurcations, i.e. unequal partition of hematocrit, are included [1,42]. Because this phenomenon depends on the flow split at each bifurcation, flow resistances depend on flow rates. A further iteration is therefore performed, until flows and hematocrits converge within a specified tolerance. The wall shear stress in each segment is computed as

$$\tau_w = D\Delta P / (4L). \quad (2)$$

Oxygen transport

At each time step, the transport of oxygen and its spatial distribution in vessels and in tissue are simulated. The oxygen field is assumed to be quasi-steady, and is computed using the Green's function method [43,44]. In the tissue, the partial pressure of oxygen, $P_{O_2}(x,y,z)$, satisfies

$$D_{O_2}\alpha\nabla^2 P_{O_2} = M(P_{O_2}) \quad (3)$$

where D_{O_2} and α are oxygen diffusivity and solubility. Michaelis-Menten kinetics are assumed for oxygen consumption rate:

$$M(P_{O_2}) = M_0 P_{O_2} / (P_0 + P_{O_2}) \quad (4)$$

where M_0 is oxygen demand and P_0 is P_{O_2} at half-maximal consumption. In blood, the convective oxygen flux is

$$f(P_b) = Q[H_D C_0 S(P_b) + \alpha_{eff} P_b] \quad (5)$$

where H_D is discharge hematocrit, C_0 is maximal RBC oxygen concentration, α_{eff} is effective oxygen solubility in blood,

$$S = P_b^n / (P_b^n + P_{50}^n) \quad (6)$$

is oxyhemoglobin saturation and P_b is blood P_{O_2} .

In the Green's function method, the oxygen field in the tissue is calculated by superposing the fields resulting from arrays of sources and sinks representing oxygen released by vessels and taken up in the tissue. The tissue is discretized as a cubic array of points spaced 20 μm apart, resulting in 3675 points. The vessel network is discretized into segments with lengths averaging about 20 μm , resulting in approximately 1000 segments in a typical simulation. The source strength of a segment is equal to the decrease in $f(P_b)$ from inlet to outlet. The source and sink strengths are computed using an iterative algorithm such that intravascular and extravascular oxygen levels match at each segment, taking into account the effects of intravascular resistance to radial oxygen diffusion [45].

Growth factor production and transport

Multiple agents are involved in angiogenesis and structural adaptation of blood vessels, including several forms of vascular endothelial growth factor (VEGF), fibroblast growth factor, tumor necrosis factor- α , transforming growth factor- β , and angiopoietins [46]. These factors have several effects, including stabilization or destabilization of the vessel wall, modulation of wall permeability, formation of sprouts, directional migration of endothelial cells, and differentiation and proliferation of vascular cells. The production of growth factors is sensitive to metabolic conditions in the tissue. In particular, VEGF is released in hypoxic regions, diffuses through tissue, and stimulates growth of new vessels [47,48].

In the present model, a single growth factor (GF) is introduced to represent activities needed for the development of functional vascular networks. Some of the assumed activities align with those of VEGF, but the assumed parameter values are not specific to VEGF. The GF represents in a simplified way the combined actions of the growth factors. It is assumed to be released throughout the tissue depending on the local oxygen level, to diffuse through the tissue and to be degraded with linear kinetics. Its concentration $C_{GF}(x,y,z)$ in tissue satisfies

$$D_{GF}\nabla^2 C_{GF} = -M_{GF} + K_{GF}C_{GF} \tag{7}$$

where D_{GF} is diffusivity and K_{GF} is degradation rate. Potential convection of GF by tissue fluid [49] is neglected. The release rate in tissue is assumed to be a decreasing function of local P_{O_2} :

$$M_{GF} = \frac{K_{GF}C_{GF0}}{1 + (P_{O_2}/P_{GF})^{N_{GF}}} \tag{8}$$

Here and elsewhere in the model, Hill-type functions are used to represent biological responses. The constant P_{GF} is the tissue P_{O_2} at half-maximal release rate and the exponent N_{GF} controls the sensitivity of the response. From these definitions, C_{GF0} is the maximal GF level that is reached when $P_{O_2} = 0$. The Green’s function method [43] is used to compute C_{GF} in the tissue domain. The effect of GF uptake by vessels is neglected in the computation of the tissue GF field.

Sprout formation

The network is assumed to grow by sprouting angiogenesis, represented using a previously developed model [6,14]. At each time step, the GF concentration C_{GF} at each segment is computed. The assumed probability of sprout formation on that segment is

$$P_{sprout} = \begin{cases} k_p l_{seg} \Delta t \frac{C_{GF} - C_{th}}{C_{th50} + C_{GF} - C_{th}} & \text{if } C_{GF} > C_{th} \\ 0 & \text{if } C_{GF} \leq C_{th} \end{cases} \tag{9}$$

where k_p is the maximal probability of sprout formation per length per time, l_{seg} is segment length, Δt is the time step, C_{th} is the threshold level of GF for sprout formation and C_{th50} determines the GF level for half-maximal sprout probability. The location of a new sprout on the parent segment is chosen randomly. If it is within 10 μm of a node, it is moved to that node, and if it is at a network boundary node or an existing branch point, it is suppressed. These rules are needed to avoid formation of very short segments and other anomalous structures. The direction of sprouting is chosen at random in the plane perpendicular to the parent segment.

Elongation of sprouts

Sprouts grow at a rate V_g and maintain a fixed diameter D_{new} until they connect with another vessel. The growth direction varies at each time step in response to three types of input: (i) random variation; (ii) “homing” to other segments; (iii) responses to GF gradients. These effects are implemented as follows. (i) To simulate the stochastic nature of vessel growth, the growth direction \mathbf{d} at the previous step is rotated through a random angle in three dimensions with variance σ_s , giving a new direction \mathbf{d}' . (ii) To allow growing sprouts to detect and connect to other segments, a homing mechanism is introduced, representing the activity of the filopodia of the tip cells leading sprout growth, which explore the tissue ahead of the sprout and may sense other vessels [50]. A conical region is defined that extends a distance R_{max} from the tip at angles up to θ_{max} from the direction \mathbf{d}' . A vector directed towards segments within this region is defined:

$$\mathbf{d}_v = \sum \mathbf{e}_s f(r) g(\theta) ds \tag{10}$$

where the sum is over the segments within the sector, the integral is along each segment, \mathbf{e}_s is a unit vector directed from the tip to the segment, r and θ describe the positions of points on each segment relative to the current tip position and orientation, and f and g are chosen to give a weighting factor that decays to zero at the edges of the region:

$$f(r) = \begin{cases} 1 - r/R_{max} & \text{if } r < R_{max} \\ 0 & \text{if } r \geq R_{max} \end{cases}, \tag{11}$$

$$g(\theta) = \begin{cases} 1 - \frac{1 - \cos\theta}{1 - \cos\theta_{max}} & \text{if } \theta < \theta_{max} \\ 0 & \text{if } \theta \geq \theta_{max} \end{cases}. \tag{12}$$

(iii) To represent the tendency of sprouts to grow up gradients of GF [14], the vector gradient ∇C_{GF} at the sprout tip is computed. The updated sprout direction is

$$\mathbf{d}'' = \mathbf{d}' + k_v \mathbf{d}_v + k_{GF} \nabla C_{GF} \tag{13}$$

where k_v and k_{GF} represent sensitivity of growth direction to existing vessels and to GF gradients.

During one time step, each sprout grows a distance $V_g \Delta t$. This is done in increments of $5 \mu\text{m}$, and a connection is created if the tip comes within $5 \mu\text{m}$ of another segment. Other adjustments are made as needed to avoid anomalous structures [6].

Tension-induced migration

The formation of sprouts as described above results in bifurcations with branching angles of 180° and 90° , whereas observed networks show a smooth distribution of branching angles clustered around 120° . This discrepancy implies that vessels must migrate through tissue after bifurcations form [6]. Blood vessels are under longitudinal tension *in vivo* [51,52] and collagen and other interstitial components are subject to turnover [53], so that vessels may migrate through the interstitium. To simulate this, the normalized force acting on each node in the network is computed, assuming that the tension in each vessel is proportional to diameter:

$$\mathbf{f}_i = \left(\sum D_i \mathbf{e}_i \right) \left(\sum D_i \right) / \left(\sum l_i D_i \right) \tag{14}$$

where the sum is over the segments at the node, D_i are diameters, l_i are lengths and \mathbf{e}_i are unit

vectors parallel to the segments. This is a modified version of the previous model [6]. At an unbranched node, $|\mathbf{f}_t|$ gives a dimensionless estimate of vessel curvature. If $|\mathbf{f}_t|$ exceeds a threshold λ_b , the node migrates with velocity

$$\mathbf{v} = v_{max} \mathbf{f}_t (1 - \lambda_t / |\mathbf{f}_t|) \tag{15}$$

where v_{max} is the maximum speed and λ_t defines the ratio of vessel diameter to threshold radius of curvature. The threshold allows stabilization of curved vessels, which would otherwise eventually straighten out.

Structural adaptation and pruning

Structural adaptation of vessel diameters is essential for the generation of functional and efficient vascular networks [6]. The present model follows previous work [40,54], but with modifications to achieve stable network structures in three dimensions. It is based on the assumption that structural change of vessel diameters occurs in response to the combined effects of four types of signals: wall shear stress τ_w , intravascular pressure P , downstream convected metabolic signal S_m and upstream conducted metabolic signal S_c . Each segment diameter D thus varies at each time step according to

$$\Delta D = S_{tot} D \Delta t / T \tag{16}$$

where Δt is the time step, T is a characteristic timescale, and S_{tot} is the dimensionless total adaptive signal:

$$S_{tot} = \log(\tau_w + \tau_{ref}) - \log \tau_e(P) + k_m(S_m + S_c) / D - k_s. \tag{17}$$

The logarithmic dependence on τ_w is included to ensure sensitivity over the observed wide range of wall shear stresses [55], including the tendency of segments experiencing low levels of wall shear stress to regress [56]. The small constant τ_{ref} is included to avoid singular behavior. The correlation of the expected shear stress τ_e (in dyn/cm²) with P (in mmHg) previously reported [40] is here fitted using a Hill-type equation

$$\tau_e(P) = 14 + 86 \frac{P^5}{P^5 + P_\tau^5} \tag{18}$$

with $P_\tau = 36$ mmHg. The present model differs from that used previously [6] in that the contributions of S_c and S_m to S_{tot} are assumed to vary inversely with D in Eq (17). Such dependence was necessary to avoid excessive dropout of small vessels while also avoiding unrealistically large diameters of main feeding and draining vessels.

Adaptive responses to metabolic needs are represented by the dimensionless signals S_m and S_c , both of which depend indirectly on tissue oxygen levels, via GF that is generated in the tissue and diffuses to vessels. The GF may enter vessels, where it is convected downstream, or it may stimulate release of other signaling substances by endothelial cells in proportion to GF level. The model is applicable to either situation. In the previous model [6], metabolic signals depended on intravascular oxygen levels, whereas in the present model, metabolic signals are generated in the tissue [57] and transmitted to the vessels by diffusion of GF (Fig 1A).

The steps in computing S_m and S_c in each segment are as follows. (i) Under the assumption that GF diffuses into each segment at a rate proportional C_{GF} , the convective flux of GF is given by

$$\frac{dJ_{GF}}{ds} = \kappa_{GF} C_{GF} \tag{19}$$

where C_{GF} is the concentration in the adjacent tissue, κ_{GF} is a permeability coefficient and s is downstream distance along each segment. The flux is initialized to zero at network inflows. (ii) The vessel GF concentration is

$$C_{GF}^v = \frac{J_{GF}}{Q + Q_{ref}} \quad (20)$$

where J_{GF} is evaluated at the midpoint of the segment, Q is flow rate in nl/min and Q_{ref} is a small constant to avoid singular behavior. (iii) The downstream convected metabolic signal is a function of concentration:

$$S_m = \frac{C_{GF}^v}{C_{GF}^v + C_{GF50}^v} \quad (21)$$

(iv) The convected metabolic signal stimulates an upstream conducted response in the vessel wall, denoted J_c which decays with distance traveled:

$$\frac{dJ_c}{ds} = S_m - J_c/L_c \quad (22)$$

where s here denotes upstream distance. The signal is initialized to zero at network outflows. At converging bifurcations relative to direction of conduction, incoming signals are weighted by the diameters of the vessels and summed. At diverging bifurcations, the outgoing signal is divided among the upstream vessels in proportion to their diameters. (v) The conducted metabolic signal is

$$S_c = S_c^{max} \frac{J_c}{J_c + J_{c50}} \quad (23)$$

where S_c^{max} controls the relative magnitudes of convected and conducted signals.

Pruning of redundant vessels is simulated by assuming that a vessel drops out if its diameter drops below $3 \mu\text{m}$, the approximate minimum for passage of red blood cells [58]. Any other segments whose flows cease as a result are also pruned.

Parameter values

Table 1 gives parameter values. Precise values are stated for computational reproducibility, but the number of decimals shown does not imply a corresponding precision in their estimates. Oxygen transport parameter values for blood and tissue are from previous studies [5,36,37]. Parameter values for GF transport, angiogenesis and structural adaptation are not generally available *a priori*. A feasible set of values (the reference parameter set) was obtained by performing many simulations to explore the parameter space and applying the following criteria. (i) The simulation converges to a stable final state within the simulation period of 10 days, which represents the time for development of cortical microcirculation [7]. Stability requires that $C_{GF} < C_{th}$ throughout the domain, so that no further sprouts are formed. (ii) In the final state, tissue $P_{O_2} > 20 \text{ mmHg}$ throughout the domain [5]. (iii) The initial A-V connection on the pial surface is pruned [7]. (iv) The final vessel length density matches that in the experimental network [5]. (v) The final oxygen extraction matches that computed for the experimental network [5]. An objective function was defined as:

$$E = F_{GF}^2 + F_H^2 + (L_t - L_0)^2 + (E_{OX} - E_{OX0})^2 \quad (24)$$

where F_{GF} and F_H are the percent of tissue points with $C_{GF} > C_{th}$ and $P_{O_2} < 20 \text{ mmHg}$ respectively, L_t and E_{OX} are the total vessel length in mm and the percent oxygen extraction, and $L_0 =$

19.2 and $E_{OX} = 26.2$ are the target values based on experimental data [5]. Minimization of this objective function strongly restricts allowable parameter sets, but the available experimental data do not permit unique identification of the unknown model parameters.

Some parameters can be fixed without loss of generality. GF concentrations are stated in arbitrary units, and the maximal concentration C_{GF0} is set equal to 1. The model results depend on the ratio of the diffusion constant D_{GF} and the degradation rate K_{GF} , and not on their individual values. The length scale defined by $L_{GF} = (D_{GF}/K_{GF})^{1/2}$ must be large enough that vessels are responsive to nearby hypoxic tissue, but short enough that vascular responses are localized to the region of hypoxia. The reference parameter values correspond to $L_{GF} = 50 \mu\text{m}$. Because J_{GF} in Eq (19) is expressed in arbitrary units, κ_{GF} is set to 1.

A time step of 0.05 day is used for simulations. The maximal probability of sprout formation ($0.22 \mu\text{m}^{-1} \text{day}^{-1}$) gives a probability less than 0.22 for sprout formation in each time step by a 20- μm segment. The assumed growth rate of sprouts corresponds to 16.65 μm per time step, and the maximum rate of migration of nodes due to vessel tension corresponds to 4 μm per time step. The characteristic time scale for structural adaptation (Eq (16)) is set to $T = 1$ day. This gives faster remodeling than the value of 4.5 days estimated for remodeling in the adult mouse [59]. These parameters values result in development of a stable network in about 5 days, comparable to the rapid development of the cerebral microcirculation in the prenatal mouse. However, the assumed timescale is not inherent in the model. Identical results on a different timescale would be obtained with a simple rescaling of the abovementioned parameters.

The threshold concentration for sprout formation is a critical parameter. If it is too low, network structures are unstable due to GF levels above threshold. If it is too high, tissue is not well oxygenated. The effects of varying this parameter are discussed below. The maximum vessel sensing distance ($R_{max} = 25 \mu\text{m}$) is similar to the observed length of endothelial tip cell filopodia in mouse brain [8]. The attraction constant for tip cells to nearby vessels is set to a high value ($K_V = 1 \mu\text{m}^{-1}$) to ensure efficient formation of connections. The threshold (λ_t) for vessel migration gives an equilibrium radius of curvature of 40 μm for a 6- μm diameter vessel.

Sensitivity analysis

The sensitivity of three key output variables (total vessel length, total blood flow rate and oxygen extraction) to the values of several model parameters was analyzed. Each parameter was varied to values above and below its reference value, by increments of between 5% and 50%. The sensitivity of output variable X on parameter p is defined as $(\Delta X/X_{ref}) / (\Delta p/p_{ref})$, where Δp is the difference between the high and low tested values of the parameter, ΔX is the corresponding change in the output variable, and p_{ref} and X_{ref} are the values under reference conditions.

Computational procedures

The simulation is implemented using the C++ language on personal computers. The most computationally demanding aspect is the calculation of the oxygen and GF fields at each time step using the Green's function method. A system with graphical processor units (Pascal Quadro GP100, NVIDIA, Santa Clara, CA) was used to accelerate this computation. Due to the randomization of sprout formation and growth direction, the simulation results vary with the seed used for the random number generator. For reported quantitative results, simulations with 8 seeds are averaged, except where otherwise noted. The execution time per time step varies from about 1 s to several minutes depending on the network complexity. A simulation with 200 time steps takes 2 hours or more. Thousands of such simulations were performed in the process of developing and refining the model. Computer codes and data files are available at <https://github.com/secomb>.

Results

An example of simulated network development is illustrated in Fig 2. During the initial phase, non-flowing sprouts branch off the preexisting arteriole and venule. The first connections between the arteriole and venule (A-V) form at about 0.5 days and start to flow. The A-V connection on the pial surface shrinks and is pruned by 1.5 days. The length of vessels in the domain reaches a maximum at about 1.5 days, declining thereafter due to pruning. A steady state of the network is achieved by 5 days.

To give a more complete view of the network geometry, four replicates of the domain are combined in Fig 3. Numerous vessels cross the boundaries of each domain, forming a

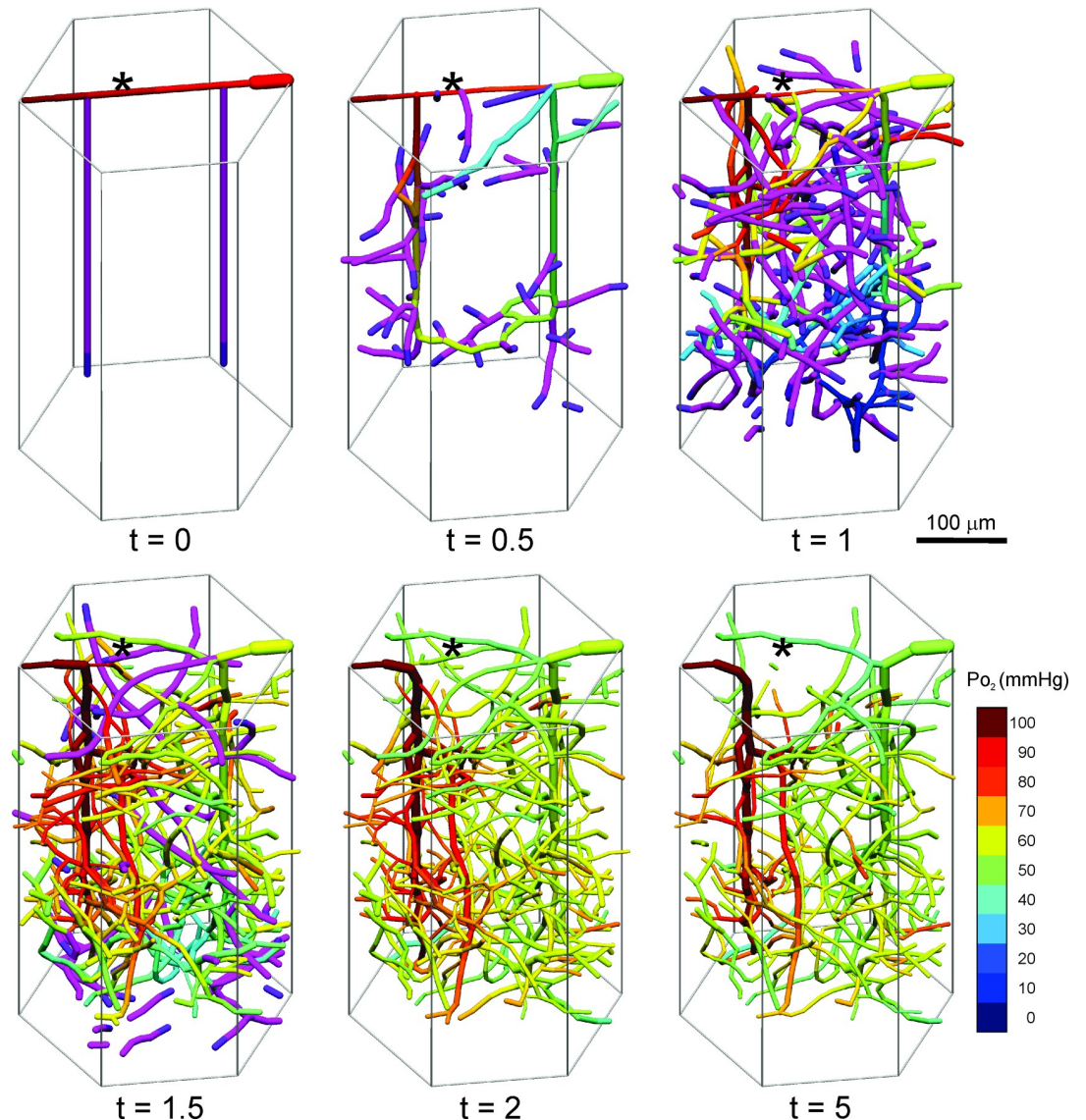


Fig 2. Example of simulated angiogenesis, remodeling and pruning. Network structure within a single hexagonal unit is shown at several time points, indicated in days. Flowing vessels are color-coded by intravascular oxygen level according to the color bar. Non-flowing sprouts are shown as purple, with tips shown as dark purple. Apparently disconnected segments are actually connected via adjacent hexagonal units. Asterisk (*) shows position of initial pial connection between arteriole and venule, illustrating shrinkage and eventual pruning of this connection, such that flow is redirected to the interior of the cortical tissue.

<https://doi.org/10.1371/journal.pcbi.1009164.g002>

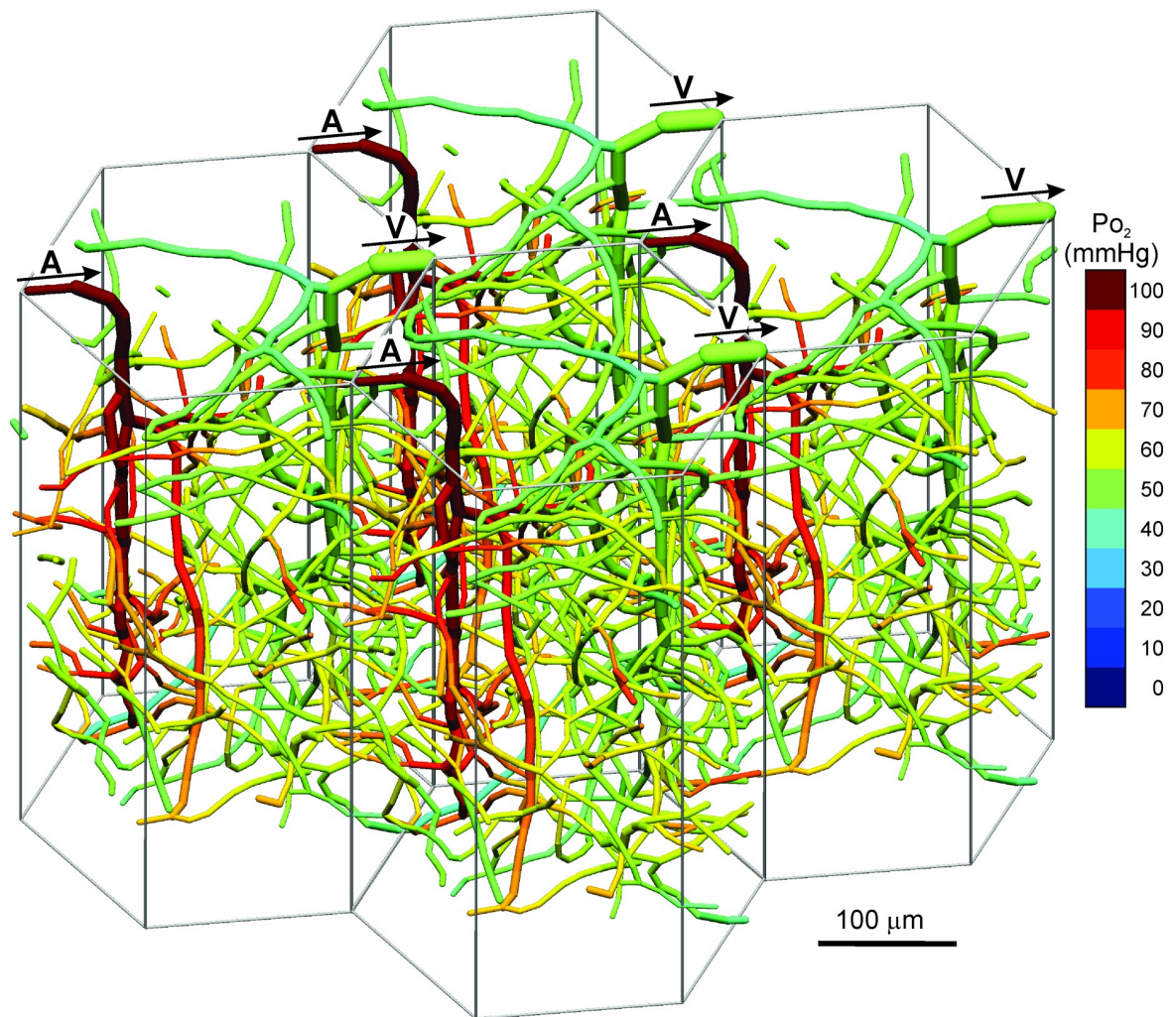


Fig 3. Final vessel configuration. Four adjacent identical hexagonal units are illustrated, to show continuity of network structure across boundaries of the hexagon. A: Penetrating arteriole. V: Penetrating venule. Arrows indicate flow direction.

<https://doi.org/10.1371/journal.pcbi.1009164.g003>

continuous mesh-like network that extends throughout the cortical layer. This structure appears similar to observed networks in the cortex of mouse [5,60] and human [33,61].

Fig 4A shows the time course of parameters describing vessel length in the simulated networks. The total length of flowing vessels starts to increase at about 0.5 days, due to the formation of A-V connections, reaching a maximum and then declining to approach a steady state. Model parameters were adjusted so that the final total length (averaged over 8 runs) corresponds to a vascular density of 658 mm^{-2} , close to the experimental value [5]. Flowing vessel segments are classified according to the types of bifurcations at their upstream and downstream ends, as “arteriolar” (diverging to diverging), “venular” (converging to converging), “capillary” (diverging to converging) and “mesh” (converging to diverging) [55]. The total lengths of all types of flowing segments reach maximal values at about 1.5 days and then decline. At steady state, mesh segments then represent about 8% of the total vascular network. Although the network appears mesh-like, this statistic indicates that the structure consists mainly of a diverging arteriolar tree connected by capillaries to a converging venular tree.

Fig 4B shows the behavior of parameters describing blood flow and oxygen transport. Blood flow rate increases initially, reaching a maximum at about 1 day, and then declines

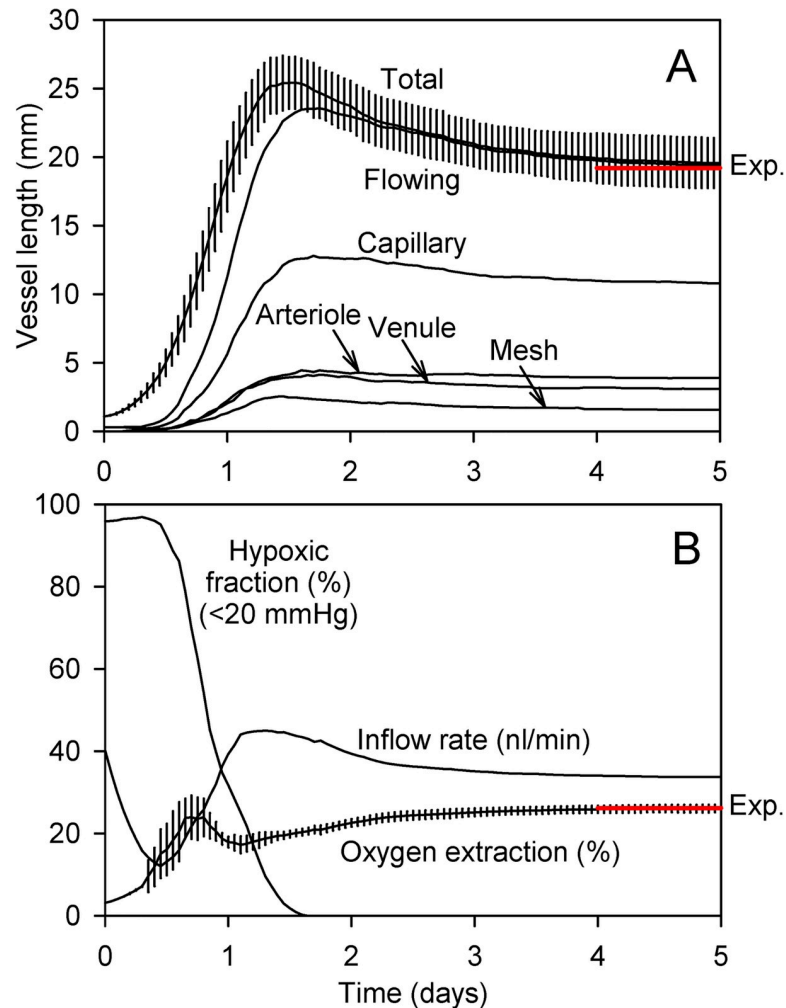


Fig 4. Dynamics of network generation. Results are the average of 8 simulations with different initial seeds for the random number generator. Vertical bars show ± 1 standard deviation. **(A)** Vessel length. Total length includes flowing vessels and non-flowing sprouts. Flowing vessels are further classified as arterioles capillaries, venules and mesh segments. Red line (Exp.): Expected vessel length based on experimentally observed length density in mouse brain cortex [5]. **(B)** Flow and oxygen transport parameters. Results for blood flow rate to the network, oxygen extraction and hypoxic fraction are shown. Red line (Exp.): Expected extraction based on simulations of oxygen transport in an experimentally observed network [5].

<https://doi.org/10.1371/journal.pcbi.1009164.g004>

slightly. The hypoxic fraction of the tissue is defined as the fraction of tissue points with $P_{O_2} < 20$ mmHg. This criterion is chosen to reflect the sensitivity of neural tissue to even moderate hypoxia. In the initial configuration, nearly all the tissue is hypoxic. When A-V connections start to form at 0.5 days, the hypoxic fraction declines, reaching zero at about 1.5 days. Oxygen extraction is defined as the A-V decrease of oxygen concentration in blood as a percent of the concentration in the inflowing arteriole. This quantity fluctuates during the initial phase, then approaches $26.27 \pm 1.06\%$ (mean \pm s.d). Model parameters were adjusted to give agreement with the value 26.2% obtained from oxygen transport simulations for the experimentally observed network [5].

Quantitative comparisons of simulated network properties with those of the experimentally observed network [5] are presented in Table 2. The perfusion (flow per volume) values match closely, as a consequence of matching oxygen extraction values and assuming the same oxygen

Table 2. Comparison of simulated networks with experimentally observed network properties.

	Observed network [5]	Simulated networks: mean \pm s.d. (n = 8)
*Total vessel length density (mm^{-2})	658.6	658.0 \pm 64.8
*Oxygen extraction (%)	26.2	26.27 \pm 1.06
Effective perfusion ($\text{cm}^3 (100\text{cm}^3)^{-1} \text{min}^{-1}$)	110.4	114.5 \pm 5.3
Mean distance of tissue points to nearest vessel (μm)	15.061	19.04 \pm 1.51
S.d. of distance of tissue points to nearest vessel (μm)	9.365	13.44 \pm 1.99
Mean vessel P_{O_2} (mmHg)	54.53	61.02 \pm 0.56
S.d. of vessel P_{O_2} (mmHg)	14.07	11.16 \pm 0.55
Mean tissue P_{O_2} (mmHg)	47.28	49.81 \pm 1.76
S.d. of tissue P_{O_2} (mmHg)	12.17	9.32 \pm 0.84

*The model parameters were adjusted to fit these two model outputs to values for the observed network

<https://doi.org/10.1371/journal.pcbi.1009164.t002>

demand. The distribution of distances of tissue points to the nearest flowing vessel strongly influences the distribution of oxygen levels. As indicated by Table 2, the simulated networks have broader distributions of this parameter (i.e. higher mean and s.d.) than the observed network, despite having the same vascular density. This may be a consequence of the relatively sparse network in the lower part of the domain (Fig 3), which results from the lack of connections to deeper vasculature. Average vessel and tissue oxygen levels are slightly higher for the simulated networks than for the observed network. Overall, the oxygen transport characteristics of the simulated networks agree approximately with those of the observed network [5].

Results of the sensitivity analysis are shown in Table 3. Because oxygen extraction varies inversely with flow rate for a given oxygen consumption rate, extraction and flow rate have approximately opposite sensitivities to each parameter. Total vessel length shows a different pattern of parameter sensitivities, with highest sensitivity to the GF threshold for sprouting (C_{th}). The value of this parameter was determined as follows. For C_{th} values below 0.6, regions with GF above threshold persisted and stable networks could not be achieved. Conversely, values above 0.8 led to persistent tissue hypoxia ($P_{\text{O}_2} < 20$ mmHg). An intermediate value of 0.7 was assumed.

Table 3. Sensitivities of total vessel length, total flow and oxygen extraction to model parameters.

Parameter	Vessel length	Total flow	Extraction
C_{th} , threshold GF concentration for sprouting	-1.080	-0.432	+0.369
k_p , maximum sprout formation probability	+0.384	+0.173	-0.155
k_{GF} , directional response to GF gradient	-0.009	-0.004	+0.006
P_{GF} , reference oxygen level for GF release	+0.703	+1.054	-0.962
N_{GF} , exponent for GF release	+0.130	-0.143	+0.144
λ_p , threshold for migration	+0.171	+0.104	-0.106
k_m , metabolic sensitivity	-0.222	+0.948	-0.888
k_s , shrinking tendency	+0.364	-1.245	+1.212
C_{GF50}^v , convected response saturation constant	-0.025	-0.549	+0.499
J_{c50} , conducted response saturation constant	-0.097	-0.282	+0.253
S_{ϵ}^{max} , relative strength of conducted response	-0.281	+0.422	-0.416

Sensitivity values with magnitude greater than 0.7 are shown **bold**.

<https://doi.org/10.1371/journal.pcbi.1009164.t003>

Two parameters whose values sensitively influence model results are the reference oxygen level for GF release (P_{GF}) and the overall metabolic sensitivity (k_m), indicating that responses to tissue metabolic status are an important component of the model. Previous studies indicate that tissue oxygen levels in the cortex under normal conditions are generally above 20 mmHg [5,62]. For the model to give this behavior, GF production rate must be sensitive to oxygen levels well above 20 mmHg. A relatively high value for the tissue P_{O_2} for half-maximal GF release is therefore required, and $P_{GF} = 40$ mmHg is assumed in the reference parameter set.

The results are insensitive to the value of k_{GF} , which defines the directional response of sprout growth to GF gradient. Directional guidance of sprout growth by VEGF gradients has been considered an important factor in angiogenesis [14], but the current simulations do not suggest a role for such guidance in the vascularization of the brain cortex.

To examine the role of metabolic responses in angiogenesis, further simulations were performed with reduced values of k_m , which determines the metabolic response including convected (downstream) and conducted (upstream) responses, and S_c^{max} , which determines the strength of the conducted response relative to the convected response. As indicated in Table 3, decreasing these parameters reduces total blood flow. To compensate for this, the parameter k_s giving the shrinking tendency of vessel diameters was adjusted in each case, so that the flow at the end of each run was within 8% of the reference value. Maintaining total flow in this way allowed assessment of the role of metabolic responses in determining the distribution of flow in the region.

Fig 5A illustrates the effects of decreasing the metabolic sensitivity k_m from its reference value ($k_m = 18$). These results are for a single run at each parameter setting. When k_m decreases below 12, mean tissue P_{O_2} declines. When $k_m \leq 7$, the pial A-V connection is not pruned, and oxygenated blood is shunted away from the underlying cortical tissue. The tissue hypoxic fraction rises sharply, and network structure does not approach a stable state. These simulations show that a structural response to metabolic signals is necessary in order to generate network structures that provide adequate tissue oxygenation to brain cortex.

The effects of decreasing S_c^{max} from its reference value ($S_c^{max} = 1$) are shown in Fig 5B. The resulting behavior is similar to that when k_m is reduced. The pial A-V connection is retained, mean tissue P_{O_2} declines, and network structure is unstable. According to these results, local and downstream convected metabolic responses are not able to maintain adequate network structures. Conducted responses propagated upstream along arterioles are essential for maintaining tissue oxygenation, as shown previously for mesenteric networks [54].

Discussion

The generation of functional microvascular networks requires angiogenesis, remodeling and pruning, which generally occur in parallel [63]. In previous work [6], we demonstrated theoretically how these processes, occurring in response to local metabolic and hemodynamic signals, can generate stable, functionally adequate structures in two dimensions, with properties matching those of observed microvascular networks in the mesentery. The present work extends the previous approach to a three-dimensional microvascular network, the vasculature of the brain cortex.

The criteria used to determine the reference parameters restrict their values but do not uniquely define them. As shown in Table 3, parameters have overlapping effects on key output variables, and equivalent results could be obtained using other combinations of parameter values. The reference parameters for angiogenesis and structural adaptation do not represent accurate estimates of actual biological effects. Indeed, such effects can be assumed to have significant natural variability. However, the objective of this work is not to determine values of

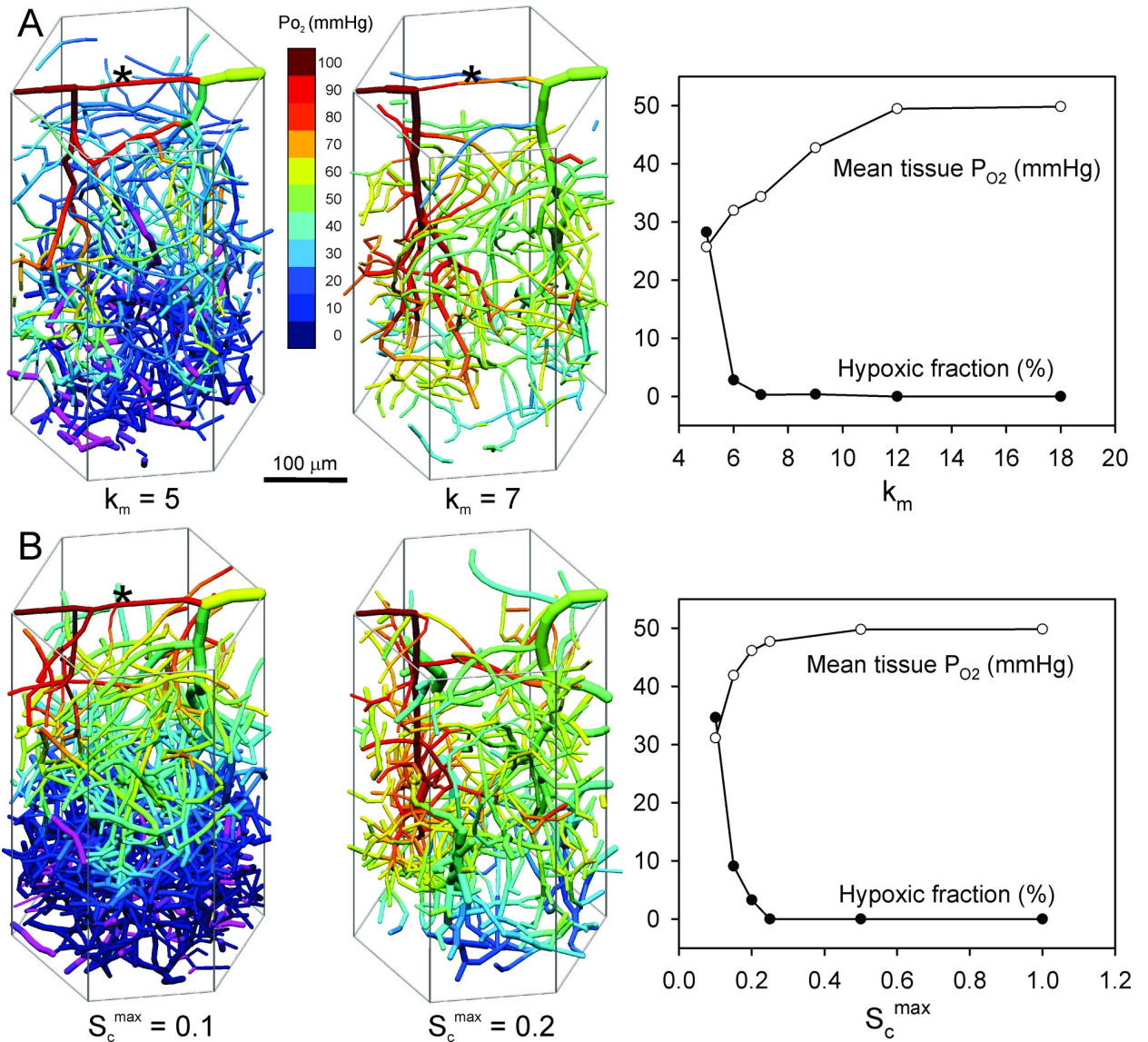


Fig 5. Effects of reduced metabolic responses. Graphs show values of mean tissue P_{O_2} and hypoxic fraction at end of simulation at 10 days (2 days for the case $S_c^{max} = 0.1$). Examples of final network structures, color-coded for vessel P_{O_2} , are shown at left of each graph. Asterisk (*) indicates retention of pial A-V connection. **(A)** Effect of reducing strength of metabolic response (k_m) while holding total flow nearly constant. **(B)** Effect of reducing relative strength of upstream conducted response (S_c^{max}) while holding total flow nearly constant.

<https://doi.org/10.1371/journal.pcbi.1009164.g005>

parameters describing angiogenesis and structural adaptation, but rather to demonstrate that networks with characteristics matching those of observed networks can be simulated by a theoretical model including the assumed set of biologically plausible mechanisms.

In the early development of the cortical microcirculation, a notable feature is the transition from a nearly two-dimensional network on the pial surface to a three-dimensional network extending through the cortical layer [7]. The present model simulates this behavior, including the loss of A-V connections on the pial surface that would otherwise shunt blood away from the interior of the cortex. The model shows the development of a continuous mesh-like network of capillaries within the cortical layer, similar to observed microvascular structures. The hexagonally periodic geometry allows the model to represent this continuous network structure (Fig 3).

The simulations permit investigation of the roles played by various response mechanisms, by varying the parameters controlling the strengths of these responses. The results confirm the importance of responses to metabolic signals in order to ensure that tissue is adequately supplied with blood flow [6]. Downregulation of these responses while maintaining overall perfusion results in impaired flow to the deeper part of the cortex, with the development of hypoxia (Fig 5A). Contributing to this behavior is the retention of the pial A-V connection under this condition. Similar behavior is predicted when only the upstream conducted response is downregulated (Fig 5B). This result indicates the essential role of conducted responses in maintaining functionally adequate network structures in the brain.

Experimental evidence supports the concept that conducted responses play an important role in the maintenance of vascular structures throughout the body. The role of conducted responses in coordinating acute vasomotor responses (i.e. flow regulation) is well established [64]. Conducted responses generated in venules have been observed to traverse the capillary bed and affect vascular tone in upstream arterioles [65]. Furthermore, chronic changes in vascular tone have been shown to lead to corresponding changes in structural vessel diameters [66,67], which implies a role for conducted responses in structural remodeling. Conducted responses are transmitted via gap junctions that connect endothelial cells. Genetic ablation of gap junction proteins in mice has been shown to affect vascular structures [68,69], a finding consistent with an essential role for conducted responses in structural adaptation.

Theoretical simulations are used to study various aspects of microcirculatory function in the brain, such as neurovascular coupling [70]. Some of these studies have been based on computer-generated synthetic capillary network structures [32,71,72], because structural information at capillary scales is difficult to obtain experimentally. Generally, these synthetic structures have been shown to be consistent with experimentally observed networks with regard to parameters such as vessel diameter and length, and surface and length densities. However, the approach presented here has advantages over previous methods for producing synthetic microvascular structures. (i) Networks are generated by algorithms that simulate known mechanisms of angiogenesis. (ii) Networks include hierarchical, tree-like arteriolar and venular structures in addition to capillaries. (iii) Blood flow and oxygen transport characteristics match predictions based on observed network structures in the mouse cortex.

The vascular component of neurodegenerative diseases is increasingly recognized but remains poorly understood [73]. Development of hypoxic micro-regions may contribute to cognitive decline in elderly people [74]. We previously proposed that the highly heterogeneous tissue oxygenation typically observed in solid tumors results from impaired conducted responses [75]. Because conducted responses depend on intact gap junctions between endothelial cells forming a continuous pathway for propagation of signals, they may be vulnerable if endothelial cells are dysfunctional. The results of the present model support the concept that reduction in conducted responses in age or disease may contribute to cognitive impairment in humans.

Author Contributions

Conceptualization: Timothy W. Secomb.

Formal analysis: Jonathan P. Alberding.

Investigation: Jonathan P. Alberding, Timothy W. Secomb.

Methodology: Timothy W. Secomb.

Software: Jonathan P. Alberding, Timothy W. Secomb.

Writing – original draft: Timothy W. Secomb.

Writing – review & editing: Jonathan P. Alberding, Timothy W. Secomb.

References

1. Pries AR, Secomb TW. Blood Flow in Microvascular Networks. In: Tuma RF, Duran WN, Ley K, editors. *Handbook of Physiology: Microcirculation* Second Edition. San Diego: Academic Press; 2008. p. 3–36.
2. Secomb TW, Hsu R, Dewhirst MW, Klitzman B, Gross JF. Analysis of oxygen transport to tumor tissue by microvascular networks. *Int J Radiat Oncol Biol Phys*. 1993; 25(3):481–9. [https://doi.org/10.1016/0360-3016\(93\)90070-c](https://doi.org/10.1016/0360-3016(93)90070-c) PMID: 8436527
3. Secomb TW, Dewhirst MW, Pries AR. Structural adaptation of normal and tumour vascular networks. *Basic Clin Pharmacol Toxicol*. 2012; 110(1):63–9. <https://doi.org/10.1111/j.1742-7843.2011.00815.x> PMID: 21995550
4. Gagnon L, Sakadzic S, Lesage F, Musacchia JJ, Lefebvre J, Fang Q, et al. Quantifying the microvascular origin of BOLD-fMRI from first principles with two-photon microscopy and an oxygen-sensitive nanoprobe. *J Neurosci*. 2015; 35(8):3663–75. <https://doi.org/10.1523/JNEUROSCI.3555-14.2015> PMID: 25716864
5. Celaya-Alcala JT, Lee GV, Smith AF, Li B, Sakadžić S, Boas DA, et al. Simulation of oxygen transport and estimation of tissue perfusion in extensive microvascular networks: Application to cerebral cortex. *J Cereb Blood Flow Metab*. 2021; 41(3):656–69. Epub 2020/06/06. <https://doi.org/10.1177/0271678X20927100> PMID: 32501155; PubMed Central PMCID: PMC7922761.
6. Secomb TW, Alberding JP, Hsu R, Dewhirst MW, Pries AR. Angiogenesis: an adaptive dynamic biological patterning problem. *PLoS Comput Biol*. 2013; 9(3):e1002983. <https://doi.org/10.1371/journal.pcbi.1002983> PLoS Comput Biol-D-12-01315 [pii]. PMID: 23555218
7. Bär T, Miodoński A, Budi Santoso AW. Postnatal development of the vascular pattern in the rat telencephalic pia-arachnoid. A SEM study. *Anat Embryol (Berl)*. 1986; 174(2):215–23. Epub 1986/01/01. <https://doi.org/10.1007/BF00824337> PMID: 3740456.
8. Wälchli T, Mateos JM, Weinman O, Babic D, Regli L, Hoerstrup SP, et al. Quantitative assessment of angiogenesis, perfused blood vessels and endothelial tip cells in the postnatal mouse brain. *Nature protocols*. 2015; 10(1):53–74. Epub 2014/12/17. <https://doi.org/10.1038/nprot.2015.002> PMID: 25502884.
9. Liotta LA, Saidel GM, Kleinerman J. Diffusion model of tumor vascularization and growth. *Bull Math Biol*. 1977; 39(1):117–28. <https://doi.org/10.1007/BF02460686> PMID: 830188
10. Balding D, McElwain DL. A mathematical model of tumour-induced capillary growth. *J Theor Biol*. 1985; 114(1):53–73. [https://doi.org/10.1016/s0022-5193\(85\)80255-1](https://doi.org/10.1016/s0022-5193(85)80255-1) PMID: 2409405
11. Anderson AR, Chaplain MA. Continuous and discrete mathematical models of tumor-induced angiogenesis. *Bull Math Biol*. 1998; 60(5):857–99. <https://doi.org/10.1006/bulm.1998.0042> PMID: 9739618
12. Hahnfeldt P, Panigrahy D, Folkman J, Hlatky L. Tumor development under angiogenic signaling: a dynamical theory of tumor growth, treatment response, and postvascular dormancy. *Cancer Res*. 1999; 59(19):4770–5. PMID: 10519381
13. Levine HA, Pamuk S, Sleeman BD, Nilsen-Hamilton M. Mathematical modeling of capillary formation and development in tumor angiogenesis: penetration into the stroma. *Bull Math Biol*. 2001; 63(5):801–63. <https://doi.org/10.1006/bulm.2001.0240> PMID: 11565406
14. Tong S, Yuan F. Numerical simulations of angiogenesis in the cornea. *Microvasc Res*. 2001; 61(1):14–27. <https://doi.org/10.1006/mvre.2000.2282> PMID: 11162192
15. McDougall SR, Anderson AR, Chaplain MA. Mathematical modelling of dynamic adaptive tumour-induced angiogenesis: clinical implications and therapeutic targeting strategies. *J Theor Biol*. 2006; 241(3):564–89. <https://doi.org/10.1016/j.jtbi.2005.12.022> PMID: 16487543
16. Owen MR, Alarcon T, Maini PK, Byrne HM. Angiogenesis and vascular remodelling in normal and cancerous tissues. *J Math Biol*. 2009; 58(4–5):689–721. <https://doi.org/10.1007/s00285-008-0213-z> PMID: 18941752
17. Welter M, Rieger H. Physical determinants of vascular network remodeling during tumor growth. *European Physical Journal e*. 2010; 33(2):149–63. <https://doi.org/10.1140/epje/i2010-10611-6> PMID: 20607341
18. Perfahl H, Byrne HM, Chen T, Estrella V, Alarcon T, Lapin A, et al. Multiscale modelling of vascular tumour growth in 3D: the roles of domain size and boundary conditions. *PLoS One*. 2011; 6(4):e14790. <https://doi.org/10.1371/journal.pone.0014790> PMID: 21533234

19. Travasso RD, Corvera PE, Castro M, Rodriguez-Manzaneque JC, Hernandez-Machado A. Tumor angiogenesis and vascular patterning: a mathematical model. *PLoS One*. 2011; 6(5):e19989. <https://doi.org/10.1371/journal.pone.0019989> PONE-D-10-06097 [pii]. PMID: 21637756
20. Vilanova G, Colominas I, Gomez H. A mathematical model of tumour angiogenesis: growth, regression and regrowth. *Journal of the Royal Society, Interface*. 2017; 14(126). Epub 2017/01/20. <https://doi.org/10.1098/rsif.2016.0918> PMID: 28100829; PubMed Central PMCID: PMC5310739.
21. Fredrich T, Welter M, Rieger H. Tumorcode: A framework to simulate vascularized tumors. *The European physical journal E, Soft matter*. 2018; 41(4):55. Epub 2018/04/28. <https://doi.org/10.1140/epje/i2018-11659-x> PMID: 29700630.
22. Pettet G, Chaplain MA, McElwain DL, Byrne HM. On the rôle of angiogenesis in wound healing. <https://doi.org/10.1098/rspb.1996.0217> PMID: 8952092 1996; 263(1376):1487–93. Epub 1996/11/22.
23. Machado MJ, Watson MG, Devlin AH, Chaplain MA, McDougall SR, Mitchell CA. Dynamics of angiogenesis during wound healing: a coupled in vivo and in silico study. *Microcirculation*. 2011; 18(3):183–97. <https://doi.org/10.1111/j.1549-8719.2010.00076.x> PMID: 21166934
24. Flegg JA, Menon SN, Maini PK, McElwain DL. On the mathematical modeling of wound healing angiogenesis in skin as a reaction-transport process. *Front Physiol*. 2015; 6:262. Epub 2015/10/21. <https://doi.org/10.3389/fphys.2015.00262> PMID: 26483695; PubMed Central PMCID: PMC4588694.
25. Murray JD. On the mechanochemical theory of biological pattern formation with application to vasculogenesis. *Comptes rendus biologiques*. 2003; 326(2):239–52. Epub 2003/05/21. [https://doi.org/10.1016/s1631-0691\(03\)00065-9](https://doi.org/10.1016/s1631-0691(03)00065-9) PMID: 12754942.
26. Ambrosi DB F.; Preziosi L. A Review of Vasculogenesis Models. *J Theor Medicine*. 2005; 6:1–19.
27. Liu G, Qutub AA, Vempati P, Mac Gabhann F, Popel AS. Module-based multiscale simulation of angiogenesis in skeletal muscle. *Theoretical biology & medical modelling*. 2011; 8:6. Epub 2011/04/06. <https://doi.org/10.1186/1742-4682-8-6> PMID: 21463529; PubMed Central PMCID: PMC3079676.
28. Watson MG, McDougall SR, Chaplain MA, Devlin AH, Mitchell CA. Dynamics of angiogenesis during murine retinal development: a coupled in vivo and in silico study. *J R Soc Interface*. 2012; 9(74):2351–64. <https://doi.org/10.1098/rsif.2012.0067> PMID: 22438490
29. Gevertz JL, Torquato S. Modeling the effects of vasculature evolution on early brain tumor growth. *J Theor Biol*. 2006; 243(4):517–31. Epub 2006/08/30. <https://doi.org/10.1016/j.jtbi.2006.07.002> PMID: 16938311.
30. Risau W. Mechanisms of angiogenesis. *Nature*. 1997; 386:671–4. <https://doi.org/10.1038/386671a0> PMID: 9109485
31. Zakrzewicz A, Secomb TW, Pries AR. Angioadaptation: keeping the vascular system in shape. *News Physiol Sci*. 2002; 17:197–201. <https://doi.org/10.1152/nips.01395.2001> PMID: 12270956
32. El-Bouri WK, Payne SJ. Multi-scale homogenization of blood flow in 3-dimensional human cerebral microvascular networks. *J Theor Biol*. 2015; 380:40–7. Epub 2015/05/20. <https://doi.org/10.1016/j.jtbi.2015.05.011> PMID: 25986433.
33. Duvernoy HM, Delon S, Vannson JL. Cortical blood vessels of the human brain. *Brain research bulletin*. 1981; 7(5):519–79. Epub 1981/11/01. [https://doi.org/10.1016/0361-9230\(81\)90007-1](https://doi.org/10.1016/0361-9230(81)90007-1) PMID: 7317796.
34. Pries AR, Secomb TW, Gessner T, Sperandio MB, Gross JF, Gaehtgens P. Resistance to blood flow in microvessels in vivo. *Circ Res*. 1994; 75(5):904–15. <https://doi.org/10.1161/01.res.75.5.904> PMID: 7923637
35. Pries AR, Secomb TW, Gaehtgens P, Gross JF. Blood flow in microvascular networks. Experiments and simulation. *Circ Res*. 1990; 67(4):826–34. <https://doi.org/10.1161/01.res.67.4.826> PMID: 2208609
36. Lucker A, Secomb TW, Weber B, Jenny P. The relative influence of hematocrit and red blood cell velocity on oxygen transport from capillaries to tissue. *Microcirculation*. 2017; 24(3). Epub 2016/11/29. <https://doi.org/10.1111/micc.12337> PMID: 27893186; PubMed Central PMCID: PMC5404950.
37. Uchida K, Reilly MP, Asakura T. Molecular stability and function of mouse hemoglobins. *Zoological Science*. 1998; 15(5):703–6.
38. Golub AS, Pittman RN. Oxygen dependence of respiration in rat spinotrapezius muscle in situ. *Am J Physiol Heart Circ Physiol*. 2012; 303(1):H47–H56. <https://doi.org/10.1152/ajpheart.00131.2012> PMID: 22523254
39. Nunes SS, Greer KA, Stiening CM, Chen HY, Kidd KR, Schwartz MA, et al. Implanted microvessels progress through distinct neovascularization phenotypes. *Microvasc Res*. 2010; 79(1):10–20. <https://doi.org/10.1016/j.mvr.2009.10.001> PMID: 19833141
40. Pries AR, Reglin B, Secomb TW. Structural adaptation of microvascular networks: functional roles of adaptive responses. *Am J Physiol Heart Circ Physiol*. 2001; 281(3):H1015–H25. <https://doi.org/10.1152/ajpheart.2001.281.3.H1015> PMID: 11514266

41. Lipowsky HH, Zweifach BW. Network analysis of microcirculation of cat mesentery. *Microvasc Res.* 1974; 7(1):73–83. [https://doi.org/10.1016/0026-2862\(74\)90038-7](https://doi.org/10.1016/0026-2862(74)90038-7) PMID: 4821172
42. Pries AR, Ley K, Claassen M, Gaehtgens P. Red cell distribution at microvascular bifurcations. *Microvasc Res.* 1989; 38(1):81–101. [https://doi.org/10.1016/0026-2862\(89\)90018-6](https://doi.org/10.1016/0026-2862(89)90018-6) PMID: 2761434
43. Secomb TW, Hsu R, Park EY, Dewhirst MW. Green's function methods for analysis of oxygen delivery to tissue by microvascular networks. *Ann Biomed Eng.* 2004; 32(11):1519–29. <https://doi.org/10.1114/b:abme.0000049036.08817.44> PMID: 15636112
44. Hsu R, Secomb TW. A Green's function method for analysis of oxygen delivery to tissue by microvascular networks. *Math Biosci.* 1989; 96(1):61–78. [https://doi.org/10.1016/0025-5564\(89\)90083-7](https://doi.org/10.1016/0025-5564(89)90083-7) PMID: 2520192
45. Hellums JD, Nair PK, Huang NS, Ohshima N. Simulation of intraluminal gas transport processes in the microcirculation. *Ann Biomed Eng.* 1996; 24(1):1–24. <https://doi.org/10.1007/BF02770991> PMID: 8669708
46. Ucuzian AA, Gassman AA, East AT, Greisler HP. Molecular mediators of angiogenesis. *Journal of burn care & research: official publication of the American Burn Association.* 2010; 31(1):158–75. Epub 2010/01/12. <https://doi.org/10.1097/BCR.0b013e3181c7ed82> PMID: 20061852; PubMed Central PMCID: PMC2818794.
47. Semenza GL. Regulation of hypoxia-induced angiogenesis: a chaperone escorts VEGF to the dance. *J Clin Invest.* 2001; 108(1):39–40. <https://doi.org/10.1172/JCI13374> PMID: 11435455
48. Ji JW, Mac Gabhann F, Popel AS. Skeletal muscle VEGF gradients in peripheral arterial disease: simulations of rest and exercise. *Am J Physiol Heart Circ Physiol.* 2007; 293(6):H3740–H9. <https://doi.org/10.1152/ajpheart.00009.2007> PMID: 17890434
49. Vilanova G, Burés M, Colominas I, Gomez H. Computational modelling suggests complex interactions between interstitial flow and tumour angiogenesis. *Journal of the Royal Society, Interface.* 2018; 15(146). Epub 2018/09/07. <https://doi.org/10.1098/rsif.2018.0415> PMID: 30185542; PubMed Central PMCID: PMC6170778.
50. Gerhardt H, Golding M, Fruttiger M, Ruhrberg C, Lundkvist A, Abramsson A, et al. VEGF guides angiogenic sprouting utilizing endothelial tip cell filopodia. *J Cell Biol.* 2003; 161(6):1163–77. <https://doi.org/10.1083/jcb.200302047> PMID: 12810700
51. Jackson ZS, Gotlieb AI, Langille BL. Wall tissue remodeling regulates longitudinal tension in arteries. *Circ Res.* 2002; 90(8):918–25. <https://doi.org/10.1161/01.res.0000016481.87703.cc> PMID: 11988494
52. Gaehtgens PAL. Radial and longitudinal distensibility of arterial microvessels in the mesentery and their dependence on extravascular structures. *Pflugers Arch.* 1971; 330(4):277–89. <https://doi.org/10.1007/BF00588580> PMID: 4947416
53. Bishop JE, Laurent GJ. Collagen turnover and its regulation in the normal and hypertrophying heart. *Eur Heart J.* 1995; 16 Suppl C:38–44. https://doi.org/10.1093/eurheartj/16.suppl_c.38 PMID: 7556271
54. Pries AR, Secomb TW, Gaehtgens P. Structural adaptation and stability of microvascular networks: theory and simulations. *Am J Physiol.* 1998; 275(2 Pt 2):H349–H60. <https://doi.org/10.1152/ajpheart.1998.275.2.H349> PMID: 9683420
55. Pries AR, Secomb TW, Gaehtgens P. Structure and hemodynamics of microvascular networks: heterogeneity and correlations. *Am J Physiol.* 1995; 269(5 Pt 2):H1713–H22. <https://doi.org/10.1152/ajpheart.1995.269.5.H1713> PMID: 7503269
56. Franco CA, Jones ML, Bernabeu MO, Geudens I, Mathivet T, Rosa A, et al. Dynamic endothelial cell rearrangements drive developmental vessel regression. *PLoS biology.* 2015; 13(4):e1002125. Epub 2015/04/18. <https://doi.org/10.1371/journal.pbio.1002125> PMID: 25884288; PubMed Central PMCID: PMC4401640.
57. Reglin B, Secomb TW, Pries AR. Structural adaptation of microvessel diameters in response to metabolic stimuli: where are the oxygen sensors? *Am J Physiol Heart Circ Physiol.* 2009; 297(6):H2206–H19. <https://doi.org/10.1152/ajpheart.00348.2009> PMID: 19783778
58. Halpern D, Secomb TW. The squeezing of red blood cells through capillaries with near-minimal diameters. *Journal of Fluid Mechanics.* 1989; 203:381–400.
59. Gruonu G, Hoying JB, Pries AR, Secomb TW. Structural remodeling of mouse gracilis artery after chronic alteration in blood supply. *Am J Physiol Heart Circ Physiol.* 2005; 288(5):H2047–H54. <https://doi.org/10.1152/ajpheart.00496.2004> PMID: 15604133
60. Blinder P, Tsai PS, Kaufhold JP, Knutsen PM, Suhl H, Kleinfeld D. The cortical angiome: an interconnected vascular network with noncolumnar patterns of blood flow. *Nat Neurosci.* 2013; 16(7):889–97. <https://doi.org/10.1038/nn.3426> PMID: 23749145
61. Reina-De La Torre F, Rodriguez-Baeza A, Sahuquillo-Barris J. Morphological characteristics and distribution pattern of the arterial vessels in human cerebral cortex: a scanning electron microscope study.

- Anat Rec. 1998; 251(1):87–96. Epub 1998/05/30. [https://doi.org/10.1002/\(SICI\)1097-0185\(199805\)251:1<87::AID-AR14>3.0.CO;2-7](https://doi.org/10.1002/(SICI)1097-0185(199805)251:1<87::AID-AR14>3.0.CO;2-7) PMID: 9605225.
62. Secomb TW, Bullock KV, Boas DA, Sakadžić S. The mass transfer coefficient for oxygen transport from blood to tissue in cerebral cortex. *J Cereb Blood Flow Metab.* 2020; 40(8):1634–46. Epub 2019/08/20. <https://doi.org/10.1177/0271678X19870068> PMID: 31423930.
 63. Pries AR, Secomb TW. Making Microvascular Networks Work: Angiogenesis, Remodeling, and Pruning. *Physiology.* 2014; 29(6):446–55. <https://doi.org/10.1152/physiol.00012.2014> PMID: 25362638.
 64. de Wit C, Wolffe SE, Hopfl B. Connexin-dependent communication within the vascular wall: contribution to the control of arteriolar diameter. *Adv Cardiol.* 2006; 42:268–83. <https://doi.org/10.1159/000092575> PMID: 16646597
 65. Collins DM, McCullough WT, Ellsworth ML. Conducted vascular responses: communication across the capillary bed. *Microvasc Res.* 1998; 56(1):43–53. <https://doi.org/10.1006/mvres.1998.2076> PMID: 9683562
 66. Bakker EN, Matlung HL, Bonta P, de Vries CJ, van Rooijen N, VanBavel E. Blood flow-dependent arterial remodelling is facilitated by inflammation but directed by vascular tone. *Cardiovasc Res.* 2008; 78(2):341–8. <https://doi.org/10.1093/cvr/cvn050> PMID: 18299286
 67. Martinez-Lemus LA, Hill MA, Meininger GA. The plastic nature of the vascular wall: a continuum of remodeling events contributing to control of arteriolar diameter and structure. *Physiology (Bethesda).* 2009; 24:45–57. <https://doi.org/10.1152/physiol.00029.2008> PMID: 19196651
 68. Simon AM, McWhorter AR. Vascular abnormalities in mice lacking the endothelial gap junction proteins connexin37 and connexin40. *Developmental biology.* 2002; 251(2):206–20. Epub 2002/11/19. <https://doi.org/10.1006/dbio.2002.0826> PMID: 12435353.
 69. Buschmann I, Pries A, Styp-Rekowska B, Hillmeister P, Loufrani L, Henrion D, et al. Pulsatile shear and Gja5 modulate arterial identity and remodeling events during flow-driven arteriogenesis. *Development.* 2010; 137(13):2187–96. <https://doi.org/10.1242/dev.045351> PMID: 20530546
 70. Moshkforoush A, Ashenagar B, Harraz OF, Dabertrand F, Longden TA, Nelson MT, et al. The capillary Kir channel as sensor and amplifier of neuronal signals: Modeling insights on K(+)-mediated neurovascular communication. *Proc Natl Acad Sci U S A.* 2020; 117(28):16626–37. Epub 2020/07/01. <https://doi.org/10.1073/pnas.2000151117> PMID: 32601236; PubMed Central PMCID: PMC7368319.
 71. Safaeian N, David T. A computational model of oxygen transport in the cerebrocapillary levels for normal and pathologic brain function. *J Cereb Blood Flow Metab.* 2013; 33(10):1633–41. <https://doi.org/10.1038/jcbfm.2013.119> PMID: 23921901
 72. Smith AF, Doyeux V, Berg M, Peyrounette M, Haft-Javaherian M, Larue AE, et al. Brain Capillary Networks Across Species: A few Simple Organizational Requirements Are Sufficient to Reproduce Both Structure and Function. *Front Physiol.* 2019; 10:233. Epub 2019/04/12. <https://doi.org/10.3389/fphys.2019.00233> PMID: 30971935; PubMed Central PMCID: PMC6444172.
 73. O'Brien JT, Thomas A. Vascular dementia. *Lancet (London, England).* 2015; 386(10004):1698–706. Epub 2015/11/26. [https://doi.org/10.1016/S0140-6736\(15\)00463-8](https://doi.org/10.1016/S0140-6736(15)00463-8) PMID: 26595643.
 74. Moeini M, Lu X, Avti PK, Damseh R, Bélanger S, Picard F, et al. Compromised microvascular oxygen delivery increases brain tissue vulnerability with age. *Scientific reports.* 2018; 8(1):8219. Epub 2018/05/31. <https://doi.org/10.1038/s41598-018-26543-w> PMID: 29844478; PubMed Central PMCID: PMC5974237.
 75. Pries AR, Hopfner M, le Noble F, Dewhirst MW, Secomb TW. The shunt problem: control of functional shunting in normal and tumour vasculature. *Nat Rev Cancer.* 2010; 10(8):587–93. <https://doi.org/10.1038/nrc2895> PMID: 20631803